

Wake-airfoil interaction as broadband noise source: a large-eddy simulation study

Jérôme Boudet[†], Nathalie Grosjean, Marc C. Jacob

Laboratoire de Mécanique des Fluides et d'Acoustique (LMFA)
Ecole Centrale de Lyon/Université Claude Bernard Lyon 1/UMR CNRS 5509
36, avenue Guy de Collongue – 69134 Ecully Cedex – France
e-mail: jboudet@surrey.ac.uk

ABSTRACT

A large-eddy simulation is carried out on a rod-airfoil configuration and compared to an accompanying experiment as well as to a RANS computation. A NACA0012 airfoil (chord $c = 0.1$ m) is located one chord downstream of a circular rod (diameter $d = c/10$, $Re_d = 48\,000$). The computed interaction of the resulting sub-critical vortex street with the airfoil is assessed using averaged quantities, aerodynamic spectra and proper orthogonal decomposition (POD) of the instantaneous flow fields. Snapshots of the flow field are compared to particle image velocimetry (PIV) data. The acoustic far field is predicted using the Ffowcs Williams & Hawkings acoustic analogy, and compared to the experimental far field spectra. The large-eddy simulation is shown to accurately represent the deterministic pattern of the vortex shedding that is described by POD modes 1 & 2 and the resulting tonal noise also compares favourably to measurements. Furthermore higher order POD modes that are found in the PIV data are well predicted by the computation. The broadband content of the aerodynamic and the acoustic fields is consequently well predicted over a large range of frequencies ([0 kHz; 10 kHz]).

NOMENCLATURE

c	airfoil chord
C	speed of sound in the medium at rest
C_s	Smagorinsky constant
d	rod diameter
e_t	total energy
f	frequency
f_0	shedding frequency
k	turbulent kinetic energy
L_{exp}	spanwise extent in the experiment ($30d$)
L_{sim}	spanwise extent in the simulation ($3d$)

[†]now Research Fellow at the University of Surrey (UK) – TFS UTC.

M	Mach number
p	pressure
q	generic field quantity
Re_d	Reynolds number based on the rod diameter
S_{ij}	strain rate tensor
St	Strouhal number of the vortex shedding ($St = f_0 \cdot d / U_\infty$, where f_0 is the frequency of the vortex shedding)
U	mean flow velocity
$\langle u \rangle$	local mean streamwise velocity
u'	rms value of velocity fluctuations in local mean flow direction
u_i	velocity component in the i^{th} direction ($i = 1:x, i = 2:y, i = 3:z$)
W_{ij}	weighting factor
x, y, z	cartesian coordinates (cf. Figure 1) (origin at airfoil leading edge)
r, θ, z	cylindrical coordinates ($x = r \cos\theta - c/2, y = r \sin\theta$) for observer point (origin at airfoil centre)
δ_{ij}	Kronecker symbol
Δ_c	filter size
$\Delta x^+, \Delta y^+, \Delta z^+$	near wall mesh spacing in wall units (tangent to wall, normal to wall and spanwise respectively)
Γ^2	correlation function
λ	bulk viscosity
μ	dynamic viscosity ($\mu = \rho\nu$)
μ_{sgs}	subgrid-scale viscosity ($\mu_{\text{sgs}} = \rho\nu_{\text{sgs}}$)
ρ	density
σ_{ij}	deviatoric part of strain rate tensor
ω	turbulent dissipation (model of Wilcox [28])

SUBSCRIPTS

∞	upstream flow quantities
----------	--------------------------

SUPERSCRIPTS

—	filter operator
\sim	Favre operator

ABBREVIATIONS

CFD	computational fluid dynamics
DES	detached-eddy simulation
LES	large-eddy simulation
PIV	particle image velocimetry
POD	proper orthogonal decomposition
PSD	power spectral density
OGV	outlet guide vanes
RANS	Reynolds averaged Navier-Stokes
rms	root mean square

1. INTRODUCTION

Many practical applications involve flows governed by both deterministic and random mechanisms. On an aircraft, examples are numerous: periodic interaction of turbomachine blades with the turbulent wakes of the upstream blade row, interaction of slat cavity tones with airfoil boundary layer and wake, etc. Since these mechanisms lead to high noise levels, they have been a major research topic for the last decades.

In aeronautics, the first studies were concerned with the deterministic part of such flows. In particular, the aeolian tones of flows around cylinders have been a popular area of interest since Strouhal's pioneering work [1]. For a single airfoil, the most common noise source is of broadband nature as soon as the oncoming flow advects non negligible turbulence. Unsteady airfoil aerodynamics have therefore been very early oriented towards turbulence/airfoil interactions (*e.g.* references [2, 3, 4, 5, 6]). The essence of these approaches is to decompose incoming turbulent flow perturbations into harmonic gusts impinging the leading edge and to predict the resulting lift fluctuations from a linear theory (Sears [5]). In the seventies, Widnall [7] and Amiet [8, 9] predicted the broadband noise spectrum for single airfoils in turbulent flows by combining these theories with acoustic analogies. These theories were then extended to non-linear interactions (Goldstein & Atassi [10]). Now efforts are spent to accompany and extend these theoretical approaches by numerical ones for more complex geometries (airfoils with slats and flaps) (*e.g.* [11]).

In parallel to Amiet's work, similar approaches were developed for the prediction of both tonal and broadband noise generated by rotating blades for turbomachinery applications. In 1974, Hanson [12] studied the noise radiated by a fan submitted to atmospheric turbulence, comparing his experiments with a spectral formulation based on measured turbulent statistics. Homicz and George [13] extended Amiet's work to rotating blades assuming the shape of the turbulent spectrum at the inlet and a lift response of the airfoil governed by an aerodynamic transfer function (depending on the turbulent wavelength). More recently, Majumdar and Peake [14] also focused on ingested atmospheric turbulence, following the work of Hanson, and formulated the influence of streamline contraction on turbulence using Rapid Distortion Theory. More recently, Glegg [15] included cascade effects into a rotor-stator interaction broadband noise model.

This kind of prediction is very useful to model both the tones and the statistics of the broadband noise radiated by turbo-engines. However, as progress is made in aircraft noise reduction, the broadband contribution of engines (fan/OGV) and of high-lift devices to the overall sound level tend to increase. Since all the state-of-the-art methods have already been applied, every new noise abatement requires more advanced and precise design tools. Because of the limits of the analytical approaches, that require simplifying assumptions about the turbulent flow and the blade geometry, numerical approaches in the time domain offer a promising alternative. As pointed out by the present authors in previous studies [16, 17], only the deterministic part of a flow is predicted by solving the Reynolds Averaged Navier-Stokes (RANS) equations that are as commonly used for aerodynamic design. The prediction of the broadband noise can be achieved by adding a stochastic model for the turbulent fluctuations, such as proposed by Bailly *et al.* [18]. However, such models are often limited to particular turbulent conditions.

Therefore, new CFD methods that were so far out of reach for aeroacoustic predictions in complex flows, have to be considered in the light of currently available computer resources as a road map for future applications in an industrial environment. This is the case of large-eddy simulation (LES), which predicts the larger turbulent structures of the flow down to the size of the spatial filter, assuming that their sound radiation dominates the lower end of the acoustic spectrum. The validity of this assumption has been shown by Seror *et al.* [19], who compared a fully resolved DNS to a LES in the case of isotropic homogeneous turbulence and showed that the subgrid scale eddies do not contribute to frequencies that are a few times smaller than the cut-off frequency. Consequently, in the present configuration an LES approach can be expected to allow the prediction of the acoustic spectrum up to a frequency of the order of the cut-off frequency, which corresponds to the smallest resolved turbulent structures. For example, Terracol *et al.* [11] applied this idea to the prediction of trailing edge noise. A large-eddy simulation was used to predict the aerodynamic sources, but was not suited for acoustic propagation due to the different numerical requirements of the aerodynamic and acoustic computations. In order to predict the far field, Terracol *et al.* computed the sources for the Ffowcs Williams and Hawkings acoustic analogy [20], or used the Kirchhoff integral equation [11] in the acoustic near field. This approach is particularly convenient for simple propagation conditions, but for more complex configurations, including complex geometries (e.g. turbo-engine nacelle) or inhomogeneous propagation media, alternative Computational Aero-Acoustics methods have to be applied. The complex geometries can be taken into account using an adapted Green function in the Ffowcs Williams and Hawkings acoustic analogy (such Green functions generally need to be estimated numerically) or using the well-known Boundary Elements Method. Also, semi-analytical solutions for propagation in tubes with varying cross-sectional area are available for ducted flows and can be coupled with the far field approaches. Finally, the linearised Euler equations allow to take into account both the complex geometries and the flow inhomogeneities, but the computational cost limits its application to the near field. Schönwald *et al.* [21] presented a review of such methods for turbo-engines.

In this context, the present study is a step towards complex multi-body configurations. The flow past an airfoil in the wake of a rod is a challenge for large-eddy simulation (LES) and a relevant configuration with regard to aeronautic applications, including both tonal and broadband noise sources.

In Section 2, the configuration, the experiment and the computational tools are described. The main results are shown and discussed in Section 3, highlighting the innovative analysis of the aerodynamic field in relation with the resulting acoustics. Finally, conclusions are drawn in Section 4.

2. METHODS AND APPROACHES

Benchmark experiment

The CFD results are compared to those of a rod-airfoil experiment reported by Jacob *et al.* [22]. The experiment is carried out in the large anechoic room of the Ecole Centrale de Lyon (10 m × 8 m × 8 m). A NACA 0012 airfoil (chord: $c = 0.1\text{m}$; thickness: 0.012 m)

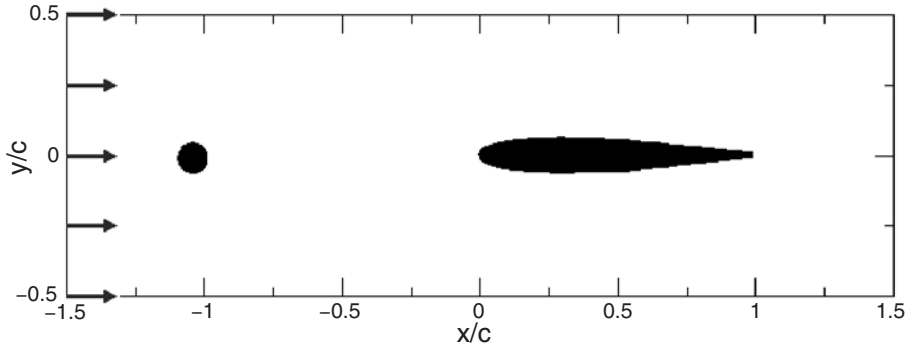


Figure 1. Rod-airfoil configuration (the origin of the axes is located at mid-span on the airfoil leading edge, and the centre of the rod is at $x = -1.04 \times c = -0.104$ m)

is located one chord downstream of a rod (diameter: $d = 0.1 \times c$), both extending over $L_{\text{exp}} = 0.3$ m in the span-wise direction. This set-up is placed into the potential core of a $U_{\infty} = 72$ m/s open rectangular jet with a $\sim 0.8\%$ turbulence level at the jet nozzle. In these conditions, the rod diameter based Reynolds number Re_d is about 48 000 and the Mach number is $M_{\infty} \sim 0.2$, giving a shedding frequency f_0 in the rod wake of about 1.3 kHz, which corresponds to a Strouhal number $St = f_0 d / U_{\infty} = 0.19$. The experimental set-up and the co-ordinates are shown in Figure 1 at a given span (z -direction). One end of the airfoil is held by a glass window for the sake of Laser Particle Image Velocimetry (PIV) measurements.

In this configuration, the rod wake that impinges the airfoil contains both periodic and broadband turbulent disturbances.

In the present study, data from single hot wire anemometry, PIV measurements, fluctuating wall pressure probes and far field microphones are compared to CFD results and to sound computations. A POD analysis of the instantaneous velocity fields is also emphasised. More details about the experimental set-up and the measurements are found in reference [22].

LES computation

The large-eddy simulation (LES) is performed with a finite volume solver based on multi-block structured grids (Proust [23]). It solves the filtered Navier-Stokes equations (1-3):

$$\frac{\partial \bar{p}}{\partial t} + \frac{\partial \bar{\rho} \tilde{u}_i}{\partial x_i} = 0 \quad (1)$$

$$\frac{\partial (\bar{\rho} \tilde{u}_i)}{\partial t} + \frac{\partial (\bar{\rho} \tilde{u}_i \tilde{u}_j)}{\partial x_j} + \frac{\partial \bar{p}}{\partial x_i} = \frac{\partial}{\partial x_j} \left[2(\tilde{\mu} + \mu_{sgs}) \tilde{\sigma}_{ij} \right] + \frac{\partial (\Pi_{kk}/3)}{\partial x_i} \quad (2)$$

$$\begin{aligned} \frac{\partial(\bar{\rho}\tilde{e}_t)}{\partial t} + \frac{\partial}{\partial x_i} [(\bar{\rho}\tilde{e}_t + \bar{p})\tilde{u}_i] &= \frac{\partial}{\partial x_j} (2\tilde{u}_i\tilde{\sigma}_{ij}) + \tilde{u}_i \frac{\partial}{\partial x_j} (2\mu_{sgs}\tilde{\sigma}_{ij}) \\ &+ \frac{\partial}{\partial x_i} \left[\left(\tilde{\lambda} + C_v \frac{\mu_{sgs}}{\text{Pr}_t} \right) \frac{\partial \tilde{T}}{\partial x_i} \right] \end{aligned} \quad (3)$$

where

$$S_{ij} = \frac{1}{2} \left(\frac{\partial u_i}{\partial x_j} + \frac{\partial u_j}{\partial x_i} \right) \text{ and } \sigma_{ij} = S_{ij} - \frac{1}{3} \delta_{ij} S_{kk}$$

$$\Pi_{ij} = -\overline{\rho u_i u_j} + \bar{\rho} \tilde{u}_i \tilde{u}_j$$

Π_{kk} is neglected according to Erlebacher [24], and v_{sgs} is modelled by the auto-adaptive model of Casalino *et al.* [16, 22, 25]:

$$v_{sgs} = C_s^2 \Delta_c^2 \sqrt{2W_{ij} \mathcal{S}_{ij}^2} \quad (4)$$

$$W_{ij} = \frac{9 \sum_{N_w} |\tilde{\mathcal{S}}_{ij}^3|}{\sum_{l,m} \sum_{N_w} |\tilde{\mathcal{S}}_{lm}^3|} \quad (5)$$

where $C_s = 0.18$, and Δ_c is the local length scale of the filter (the cubic root of the cell volume). \sum_{N_w} corresponds to the summation over the 27 nearest points that surround each mesh point, the grid being a 3D structured mesh with additional planes for the boundary conditions. This model is based on the Smagorinsky model [26], but includes the factor W_{ij} to damp the strong gradients in the regions of high mean shear: for example near the wall, where the Smagorinsky model is too dissipative, the weight factors tend to zero following the van Driest law [27]. More information about the construction of this model and its validation (channel flow, isolated rod) can be found in the references [16, 22, 25].

The fluxes are interpolated by centred spatial schemes. A 4th order scheme is used for the convective fluxes, with a 4th order artificial dissipation defined by:

$$F_{i-1/2}^{AD} = \frac{\varepsilon}{38} \times (|u| + C) \times (-6q_{i-2} + 13q_{i-1} - 13q_i + 6q_{i+1})$$

$$\varepsilon = 0.1 + \frac{0.11}{\pi} \left(\arctan(50 \times (|x| - 0.2)) + \arctan(50 \times (|y| - 0.1)) \right)$$

for the interface between points $(i-1)$ and i , where: $|u|$ is the velocity in the considered direction of the flux, C the speed of sound and q the considered field quantity on the four point stencil $(i-2$ to $i+1)$. This numerical viscosity creates a peripheral damping zone,

but vanishes for $|x| \leq 2c$ and $|y| \leq c$ in order to preserve the turbulent fluctuations. A 2nd order scheme is used for the diffusive fluxes [23]. Time marching is explicit with a 5-stage Runge-Kutta algorithm [23].

The central part of the grid is shown on Figure 2: it extends over $100d$ and $50d$ in the stream-wise (x) and cross-stream (y) directions respectively, and over $L_{sim} = 3d$ in the span-wise direction (z). The rod and the airfoil surfaces are meshed with 205 and 353 circumferential points respectively, at each span-wise location, and with 31 points along the span. The total number of points is about 2.4 million, divided into 32 grid blocks. On the airfoil, the grid density is characterised by: $\Delta x^+ < 300$ (< 85 for $x/c < 0.13$, *i.e.* in the leading edge region), $\Delta y^+ < 1.25$ and $\Delta z^+ < 350$, in the stream-wise, normal-to-wall and span-wise directions respectively. The resolution in the span-wise direction is quite low compared to wall flow scales, but since the turbulence is governed by the vortex shedding, which induces a strong correlation along z (the two-point pressure correlation length is about $3d$ on the side of the rod [16]), this spacing (31 points per correlation length) is physically reasonable.

Boundary conditions are non-slip at the walls and non-reflecting on the outer boundaries (combined with a damping layer characterised by increased numerical viscosity and grid stretching), whereas a slip condition is applied to the planes limiting the span. This latter condition has been chosen to reduce the constraints on the flow field. Unlike periodicity conditions that fully correlate all the aerodynamic field quantities of the limiting planes, the slip condition only imposes one component of velocity (z -component) to vanish and only affects the vicinity of the boundary. This condition is also physically relevant: the mean value of the spanwise velocity is zero in the modelled flow. In a previous computation [16, 25], the two-point span-wise pressure correlation on the isolated rod was proven to match the experimental one, which is of major importance for the acoustic computations and cannot be achieved with a periodicity condition. Consequently, the slip condition allows a better comparison with the experiment that was carried out with a long span ($L_{exp} = 30d$).

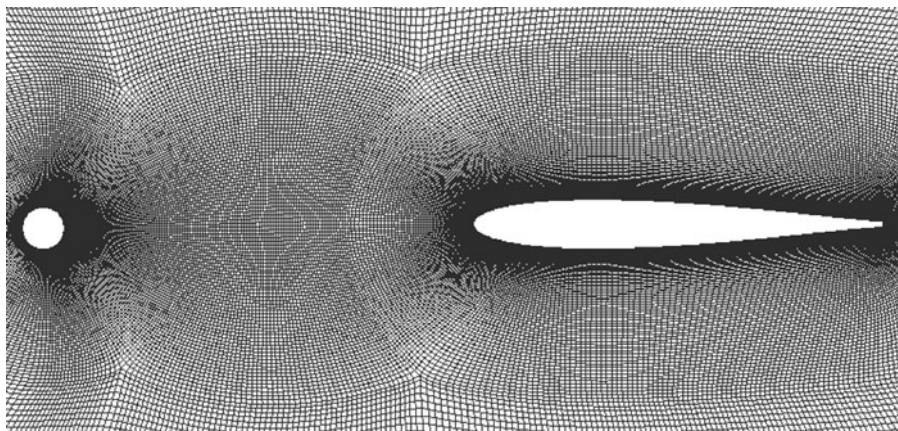


Figure 2. Detail of the LES grid

The inflow is uniform in the inlet section, and the surrounding jet flow of the experiment is not modelled. This is justified by the fact that the experimental rod-airfoil configuration was located in the potential core of the jet and that a few diameters away in the cross-stream direction, the flow became uniform over several rod diameters before the jet shear layers were reached.

The LES computation is launched from a converged RANS computation (cf. next sub-section), run over 6 cycles for further convergence and then recorded for 18 cycles.

As an example, the z -component of the instantaneous vorticity obtained from the LES computation is mapped in Figure 3. The main vortices shed from the rod (von Kármán vortices) impinge onto the airfoil and partly split at the leading edge. The airfoil wake can also be distinguished. Moreover, many smaller structures can be noticed in the rod wake, due to the transition to turbulence in the shear layers of the rod. This multiple scale flow dominated by the large von Kármán vortices is a characteristic feature of the rod-airfoil configuration in the sub-critical shedding regime.

Unsteady RANS computation

An unsteady RANS computation has been previously carried out [17], using the same code and the k - ω turbulence model of Wilcox [28] (with an inflow turbulence level $u'/U_\infty \sim 0.8\%$). The grid was only two-dimensional, because a three-dimensional configuration similar to the LES one gave no difference with the 2D grid: the flow was a span-wise repetition of the 2D flow. This is due to the averaged formulation of the RANS approach that does not predict turbulence as a fluctuating field and dampens out small perturbations. The RANS computation was considered converged when the pressure oscillations became periodic within $\pm 3\%$. This computation is compared to the LES.

Aeroacoustic computations

The rotor noise code *Advantia* (Casalino [29]) is used for the acoustic prediction. This code is based on the Ffowcs Willams & Hawkings analogy [20]. In the present

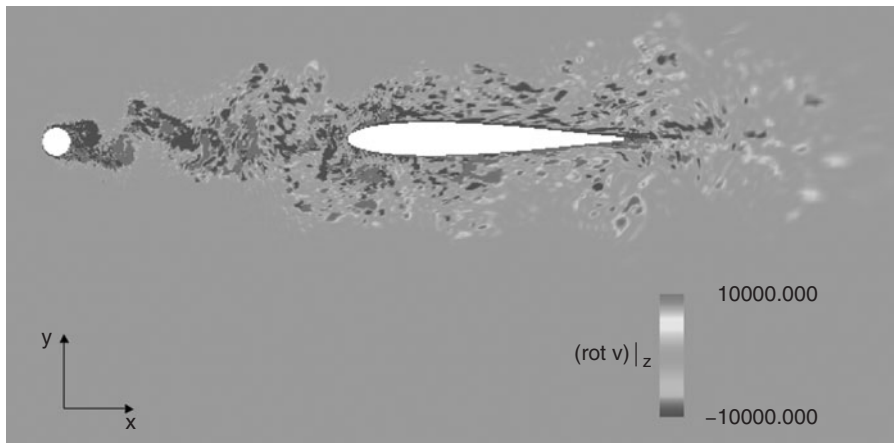


Figure 3. z -component of instantaneous vorticity from the LES computation

investigation it exploits the retarded time penetrable FW-H formulation proposed by Brentner & Farassat [30]. Only surface integrals are computed, since at the current Mach number, the volume sources give a vanishing contribution to the acoustic radiation. The consistency of this approximation has been checked by Casalino *et al.* [31] for a RANS computation of the rod-airfoil flow by comparing acoustic results obtained from different integration surfaces.

In the present paper, results are shown for a penetrable surface that surrounds the airfoil at a distance of one rod diameter (d), and is defined on the CFD mesh points. Preliminary studies such as references [16, 25] as well as experimental results [22] have shown that the rod contribution to the overall sound level is negligible with respect to that of the airfoil. This surface contains the largest eddies of the flow around the airfoil. At the shedding frequency $f_0 = 1.3$ kHz, the average surface resolution is of 356 points per wavelength in the circumferential direction, and 262 points per wave-length in the span-wise direction. At 10 kHz, these values drop to 48 and 34 respectively.

3. RESULTS AND DISCUSSION

In this section, typical results are discussed, first the velocity statistics, then the unsteady fields (spectra) and instantaneous values, and finally the far field.

Velocity statistics

Velocity statistics are compared to single hotwire data: the mean velocity modulus $\langle u \rangle / U_\infty$ and the corresponding rms velocity fluctuations in the local mean flow direction u' are plotted in Figure 4 and Figure 5 for two cross sections.

Figure 4 shows the profiles in the far rod wake at $x/c = -0.255$, that is about 7.5 rod diameters downstream of the rod. The LES provides a much more accurate description of the mean velocity than the RANS computation. The narrower and smaller velocity deficit in the RANS computation is due to the fact that separation on the rod is delayed as discussed in [16, 25]. Moreover on the LES predicted rms profile, the two mixing layers have merged similarly to the experiment, whereas they are still distinct with higher maximal values in the RANS computation. In fact the RANS profile is quite close to that predicted by potential flow. This seems to indicate that the turbulent diffusion is underestimated in the RANS computation. Both computations predict slightly higher levels than the measured ones. In the case of LES, this may be inferred to a lack of time series resulting in poorly converged statistics.

Figure 5 is dedicated to the section $x/c = 0.25$ near the airfoil thickest cross-section. Again, LES is much more accurate than RANS. In particular, the mean flow near the wall fits better to the hotwire data. The near wall region extends up to about $y/c = 0.45$ in the LES whereas it is confined to $y/c \leq 0.3$ in the RANS profile, with a pronounced maximum near $y/c = 0.18$. The shape of these profiles can be explained by the fact that in this region the flow is the result of two tendencies: on one hand the influence of the airfoil onto the steady flow is to accelerate it; on the other hand the fluctuating flow is dominated by vorticity shed from the corresponding side ($y = +d/2$) of the rod that tends to accelerate the flow away from the airfoil (the effect is strongest at the limit of the vortex core) and to slow it down near the wall. Again, the underestimated diffusion in

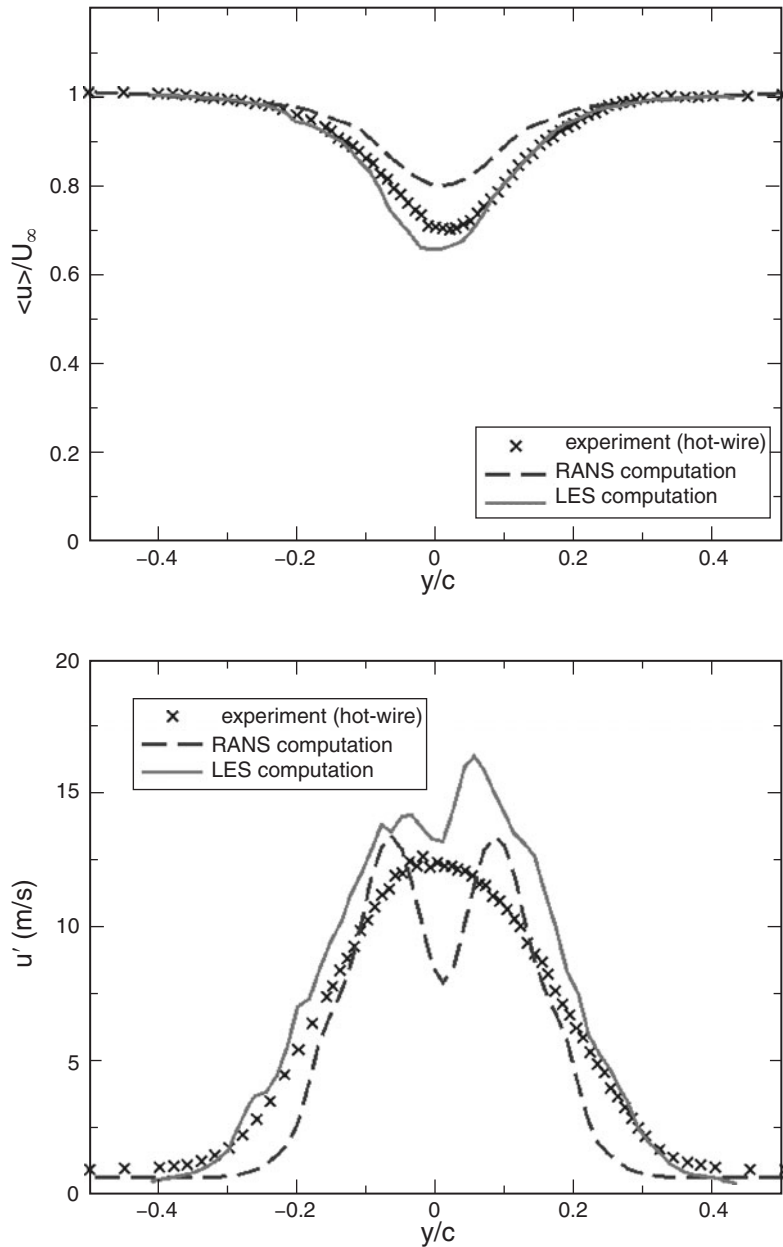


Figure 4. Mean velocity (top) and rms value of fluctuating velocity (bottom) at $x/c = -0.255$ (mid span $z=0$). [Note: for the RANS computation, $u' = \sqrt{\langle (\bar{u} \cdot \bar{n} - \langle u \rangle)^2 \rangle + 2/3 \times \langle k \rangle}$ where \bar{u} is the resolved velocity, $\bar{n} = \langle \bar{u} \rangle / \langle u \rangle$ is the mean flow direction, k the turbulent kinetic energy and $\langle \rangle$ the time average]

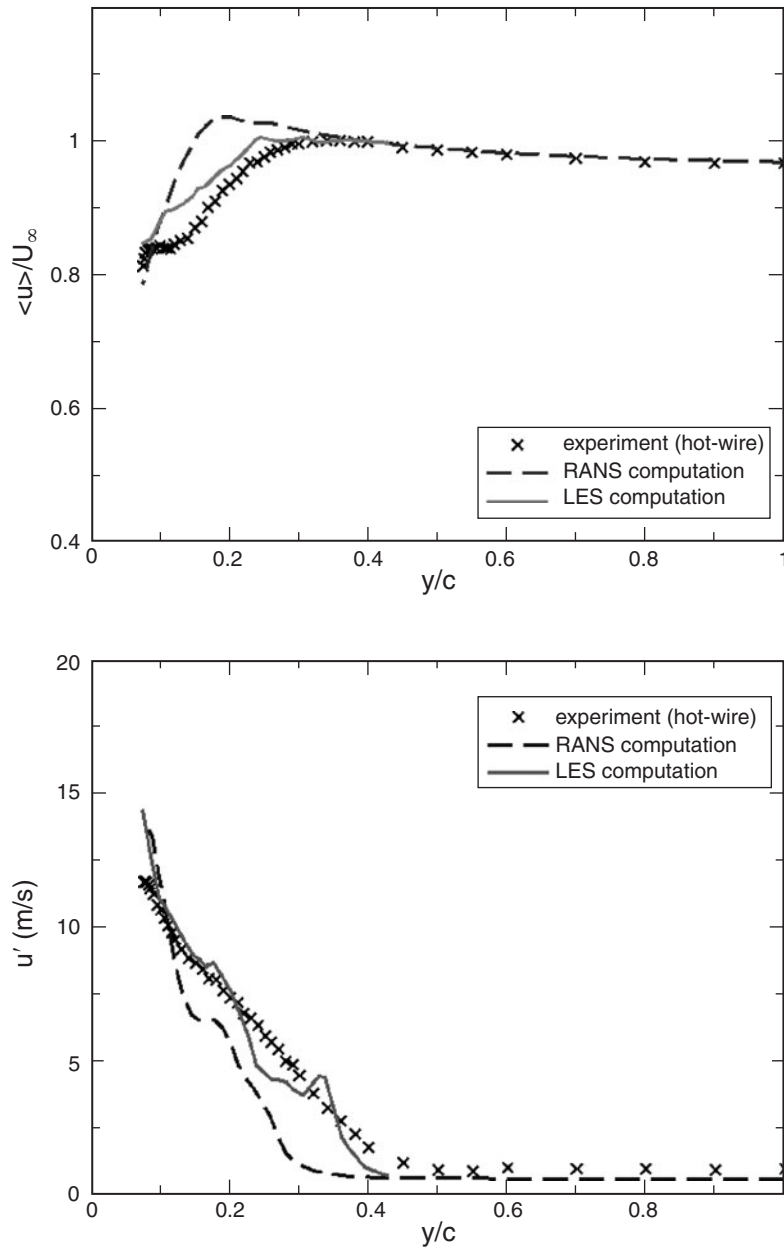


Figure 5. Mean velocity (top) and rms value of fluctuating velocity (bottom) at $x/c = 0.25$ (mid span $z=0$). [Note: for the RANS computation, $u' = \sqrt{\langle (\vec{u} \cdot \vec{n} - \langle u \rangle)^2 \rangle + 2/3 \times \langle k \rangle}$ where \vec{u} is the resolved velocity, $\vec{n} = \langle \vec{u} \rangle / \langle u \rangle$ is the mean flow direction, k the turbulent kinetic energy and $\langle \rangle$ the time average]

the RANS results in a more concentrated vorticity and therefore the effect is stronger for this computation. In the RANS solution, the well-organised vorticity patterns also result in locally high fluctuation levels that do not reach so far out into the flow as they do in the LES or in the experiment. Other evidences of this analysis will appear in the spectral analysis and in the instantaneous snapshots.

Spectral analysis of the aerodynamic fields

Another insight into this flow can be gained from the analysis of typical spectra, which are expected to distinguish the broadband from the deterministic part of the fluctuations. Thus the spectrum obtained from a wall pressure probe located at $x/c = 0.2$ on the surface of the airfoil, is plotted in Figure 6 and compared to the corresponding LES and RANS results.

All lines are dominated by the Strouhal peak of the rod shedding frequency. In the experiment this frequency is $f_0 = 1\,370$ Hz, that is $St = f_0 d/U_\infty = 0.19$. This value of St agrees with the values found in literature about vortex shedding from a circular cylinder near $Re_d \sim 4.8 \times 10^4$ [32]. On the experimental curve, the first harmonic can also be distinguished although it hardly peaks out of the background noise. The second main feature of this spectrum is the twofold influence of sub-critical rod wake turbulence: it broadens the main peak around the shedding frequency as a result of the interaction between the large von Kármán vortices and the multiple turbulent scales, and also

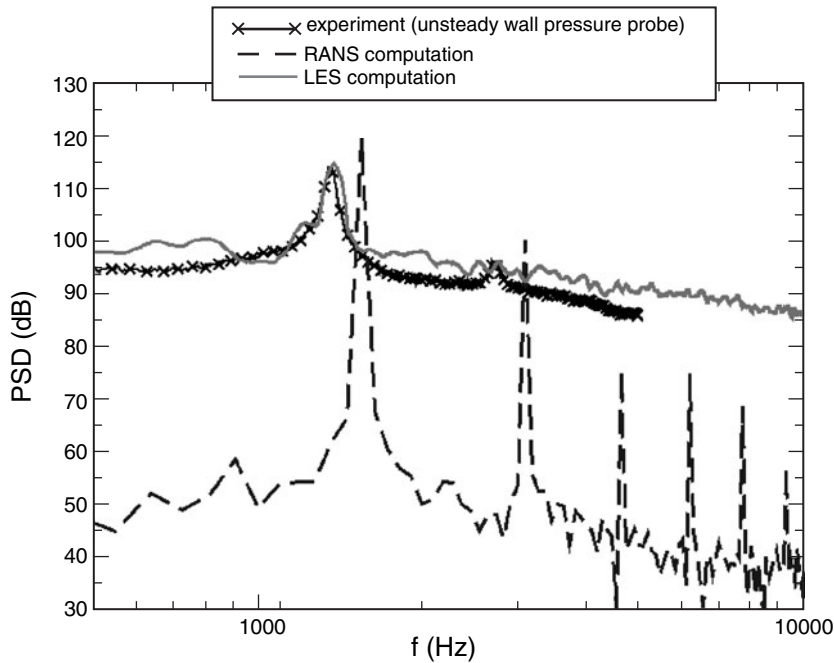


Figure 6. Pressure spectrum at $x/c = 0.2$ on the airfoil

generates a broadband spectrum that is directly related to the flow turbulence and that decays slowly in the higher frequency range.

The level and the width of the peak, as well as the background turbulent spectrum are well predicted by LES. This remarkable result shows that the LES gives an accurate flow picture of both the deterministic and the random part of the flow, even near the curved airfoil. Only the first harmonic does not clearly peak out of the broadband spectrum as it does in the experiment.

Technically, the experimental spectrum results from the average of the spectra calculated on 200 samples and has a spectral resolution of 4 Hz. This is unaffordable for the LES due to the prohibitive computational time that would be required in this explicit time approach. The present LES spectrum was obtained by averaging 31 single point spectra over the span-wise direction and has a resolution of 72 Hz.

Finally, the quality of this LES spectrum is also highlighted by the comparison with the RANS results.

The RANS spectrum in Figure 6 confirms the purely periodic deterministic nature of this flow. There is no broadband component due to turbulence since turbulence is only modelled by the averaged quantities k and ω . Furthermore, the shedding frequency is overestimated by 25%, because of the inaccurate representation of the sub-critical separation on the rod [16, 25] (delayed separation).

An example of velocity spectra at $x/c = 0.25$ is shown on Figure 7: for practical reasons the LES spectrum, which had to be chosen on the Ffowcs Williams & Hawkings integration surface, is obtained at $y/c = 0.20$ and compared to the nearest hot-wire measurements at $y/c = 0.16$ and $y/c = 0.30$ whereas the RANS spectrum is not

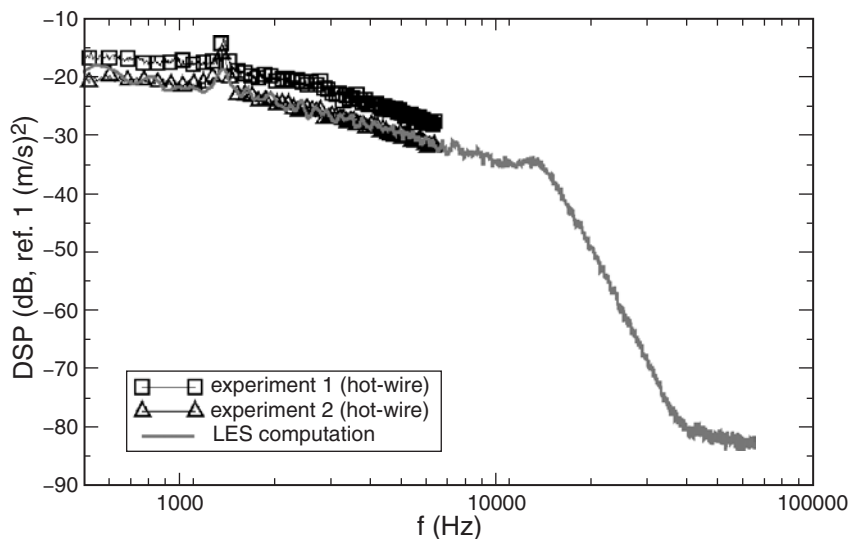


Figure 7. Velocity spectrum (experiment 1: $x/c = 0.25$ and $y/c = 0.16$; experiment 2: $x/c = 0.25$ and $y/c = 0.3$; LES: $x/c = 0.25$ and $y/c = 0.2$)

plotted here. The LES and hot-wire spectra compare very favourably. Only the level is not accurately predicted since the furthest measurement point gives the results closest to the computed ones. This indicates that the rod vortices are closer to the airfoil in the computation than in the experiment (cf. POD analysis, in the next sub-section). Besides this aspect, conclusions about this figure are essentially the same as for the wall pressure spectra. This plot also shows that the cut-off frequency of the LES filter is about 12 kHz, which is of the same order of magnitude as the local eddy turnover frequency (~ 7.5 kHz) based on the mesh size (10^{-3} m) and the rms value of the velocity fluctuations (7.5 m/s). This result confirms the high quality of the LES results already mentioned about the wall pressure spectra.

Instantaneous flow and POD analysis

A more direct insight into the flow structures can be obtained from two-dimensional vorticity snapshots extracted from the PIV and the computations. Snapshots of the z -vorticity near the airfoil leading edge are plotted in Figure 8. The same post-processing [22] tools are used for the PIV, RANS and LES fields. The LES compares remarkably well with the PIV. Large structures that are remainders of the von Kármán vortices, impact the leading edge and are partly split but mostly deviated to one side of the airfoil (the same side as they originate from, on the rod). Moreover, a variety of smaller structures that characterises the high turbulence of the experiment is also obvious in the LES flow. The topology of the wake and the levels are accurately represented by the LES. As expected, the snapshot confirms that RANS only predicts the periodic von Kármán vortices that are arranged in a stable deterministic vortex street.

A sequence of 500 snapshots is used to carry out a Proper Orthogonal Decomposition (POD), and to analyse the flow field through the extracted modes. The same POD technique [33, 22] has been applied to both the experiment and the computations. The mean flow has been subtracted from total fields; therefore the mode 0 which contains the steady part of the flow is not mentioned hereafter. The POD eigenvalues, which are proportional to the energy of the corresponding modes, are shown in Figure 9. The velocity vectors of the first POD modes are plotted in Figure 10. The agreement between LES and PIV is again striking. The first two modes carry most of the flow energy (Figure 9). They correspond to the convection of the von Kármán vortices toward the leading edge and their interaction with it (Figure 10). Since the mean field is removed from the modes, the vortices are shifted towards the axis. Considering both modes 1 and 2, the approaching vortices appear in better alignment with the x -axis in the LES than in the PIV. However, the difference lies within the spatial resolution. Because of the alignment with the x -axis, the vortices split in two at the leading edge. It is interesting to note that downstream of the leading edge, the LES modes sweep closer past the airfoil than the experimental ones, as have been inferred from the velocity spectrum in Figure 7. The third mode corresponds to a symmetric entrainment by the wake: the opposite signs of the PIV and LES modes are a mathematical artefact due to an independent choice of the modal basis. The fourth mode shows the upstream potential influence of the airfoil and the resulting deviation of the flow. Finally, the fifth mode is another vortical mode that can be related to the first two modes. This is quite surprising

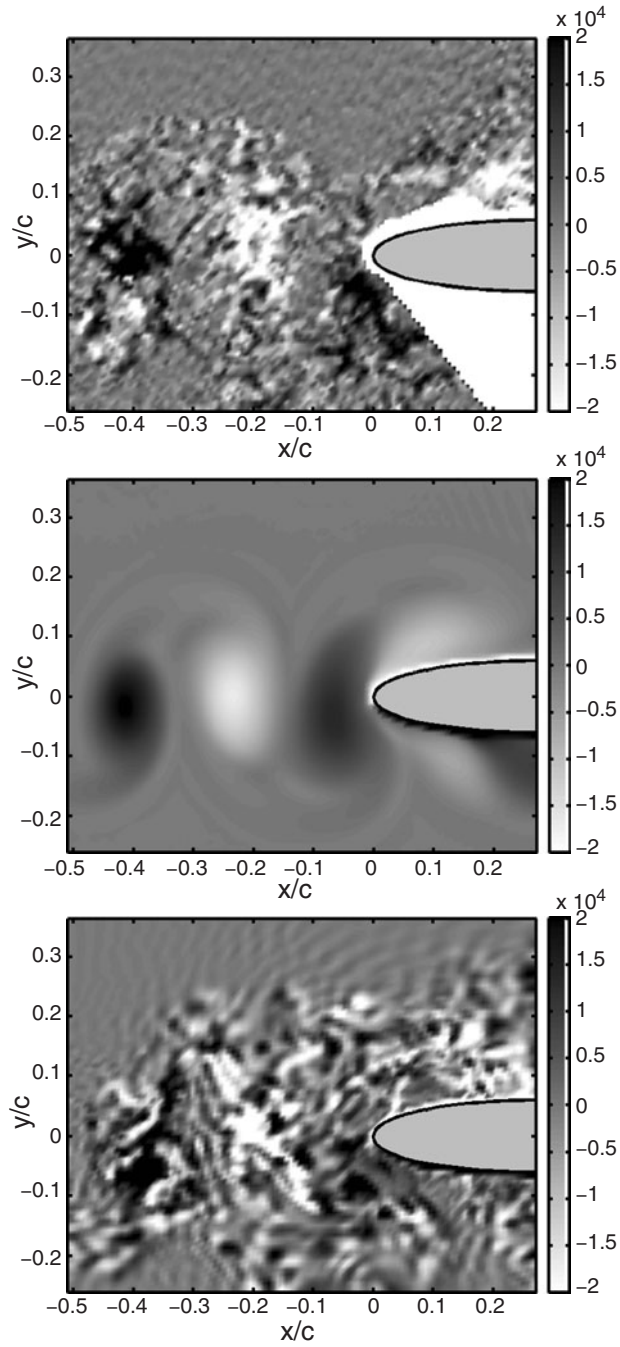


Figure 8. Instantaneous fluctuating z -vorticity near the airfoil leading edge (top: PIV measurements, middle: RANS, bottom: LES)

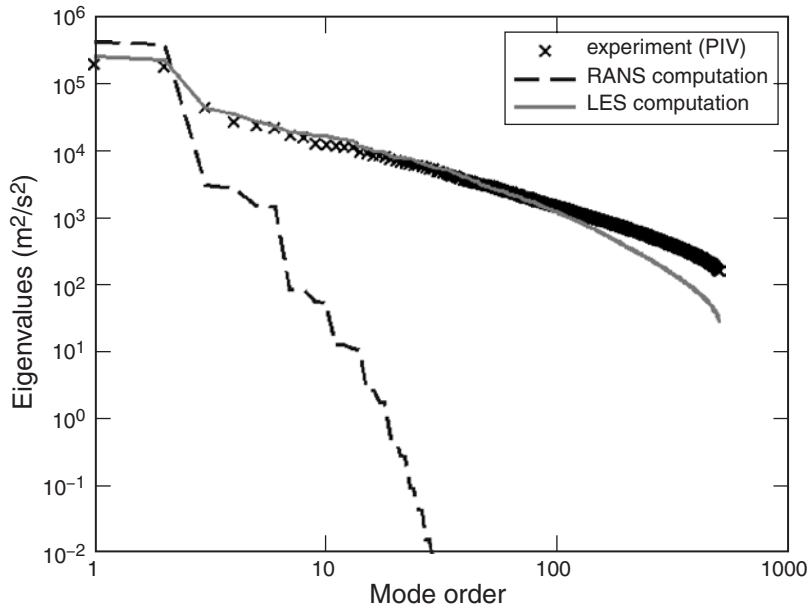


Figure 9. Eigenvalues of the POD decompositions

because higher order modes are generally not so well-organised. A possible interpretation is that this mode illustrates the interaction between the von Kármán vortices and the turbulence. These first five modes are accurately represented by the LES in terms of both shape and energy (eigenvalues). The following modes are not shown here, because of their very limited contribution to the overall energy. However, Figure 9 shows that the energy decay is very accurately predicted for the first 100 modes. In the case of RANS, all the energy is concentrated in the first two modes, which correspond to the large von Kármán vortices whereas the higher order modes (≥ 3) are negligible and their energy decay is steep. Therefore the energy of the two first modes is higher than in the experiment. This can be related to the periodic nature of the flow as discussed in the previous sections (*e.g.* the pressure spectrum in Figure 6 and the regular pattern of the instantaneous RANS vorticity field in Figure 8). The corresponding RANS modes are not shown for the sake of brevity: they are extensively discussed in reference [16]. In particular it is demonstrated that they agree fairly well with the two first PIV modes. This shows that in the POD analysis, the deterministic unsteadiness is described by the two first modes, whereas the other features of the turbulent flow are depicted by the higher order modes.

Tonal and broadband noise generation

The measured and computed acoustic far field spectra are plotted on Figure 11 at $r = 1.85$ m from the airfoil centre and $\theta = 70$ deg to the main flow direction. As mentioned in the first section, the sound computations have been carried out using the Ffowcs

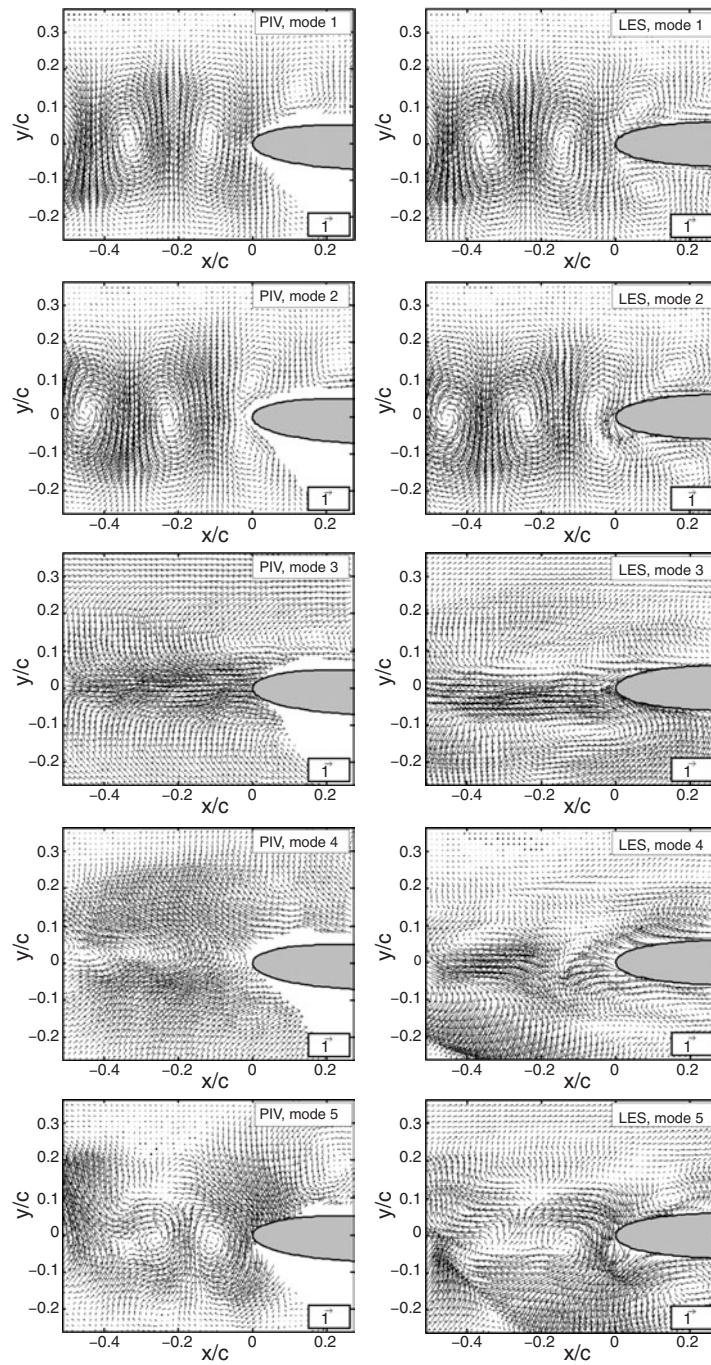


Figure 10. POD modes velocity vectors (left: PIV measurements, right: LES)

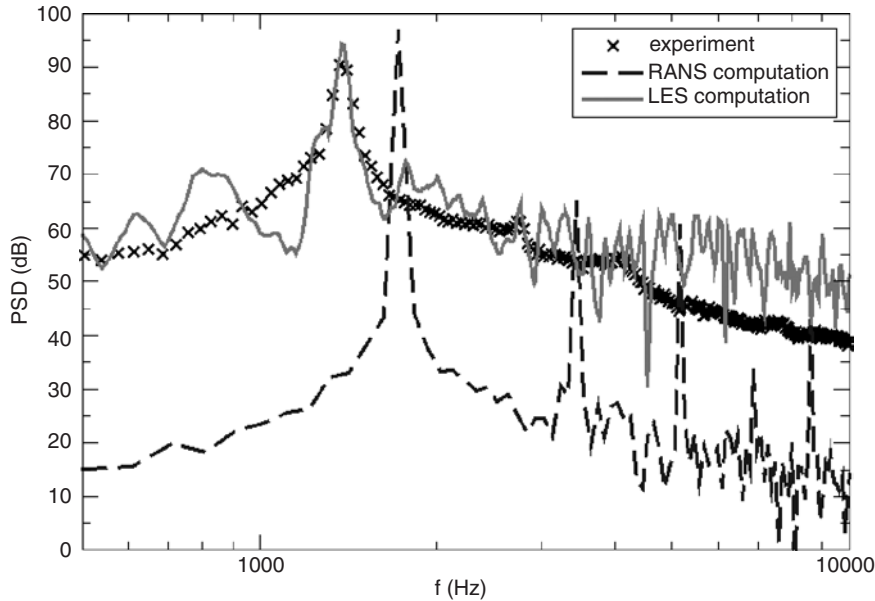


Figure 11. Power spectral density of the pressure, at $r = 1.85$ m and $\theta = 70$ deg ($x = 0.68$ m, $y = 1.74$ m)

Williams & Hawkings [20] acoustic analogy, implemented in *Advantia*. The radiation of the isolated rod is shown to be negligible compared to the rod-airfoil configuration, according to both the experimental [22] and computational [16] results. More precisely, these studies show that the spectrum of the rod is about 10 dB lower than that of the rod-airfoil configuration. Therefore, the numerical integration is carried out on a penetrable control surface surrounding only the airfoil, at a distance $1d = 0.1c$ from the physical surface, and no volume integration is performed. This approach is computationally less expensive than a volume integration, and takes into account both the surface sources on the airfoil and the volume sources resulting from the interaction of the rod wake (typical extent: $2d$) with the airfoil. In the present case, the instantaneous snapshots (Figure 8) and the main POD modes (Figure 10) show that the largest vortical perturbations remain generally in the vicinity of the wall as they are convected along the airfoil. As a result the surface sound sources and the main volume sound sources are taken into account.

Another concern is the influence of the span. The LES has been carried out for a $L_{\text{sim}} = 3d$ span, whereas the experimental facility had a span of $L_{\text{exp}} = 30d$. In order to compare the LES results to the experimental data, a correction of the LES data that takes into account the span-wise coherence must be applied. The LES span-wise pressure correlation on the isolated rod was proven to match the experimental one [16, 25] (no experimental data are available for the airfoil) and can be considered as a reasonable estimate for both the rod and the airfoil due to the persistence of the

main vortices. Hence the span-wise pressure coherence computed on the rod was preferred to correct the power spectral density according to the formula:

$$PSD(f) = PSD_{LES}(f) + 10.0 \times \log \left\{ \frac{\int_{-L_{exp}/2}^{L_{exp}/2} \int_{-L_{exp}/2}^{L_{exp}/2} \Gamma(f, \Delta z) dz_1 dz_2}{\int_{-L_{sim}/2}^{L_{sim}/2} \int_{-L_{sim}/2}^{L_{sim}/2} \Gamma(f, \Delta z) dz_1 dz_2} \right\} \quad (6)$$

where $\Gamma^2(f, \Delta z)$ is the coherence at the frequency f , between two points separated by the span-wise distance Δz along the rod, PSD_{LES} is the power spectral density provided by LES and PSD the corrected value. More information about this correction that fully relies on LES data can be found in references [16, 25].

For the sound computation based on the RANS prediction, the two-dimensional flow field is simply repeated in the span-wise direction over $30d$, assuming the flow field to be fully correlated. This gives the sound field as it can be derived by relying only on the data provided by the RANS computation. Casalino *et al.* [31, 22] showed that a much more realistic far field can be predicted from a RANS computation if the stochastic nature of the vortex shedding is modelled on the basis of experimental data about the span-wise correlation and if the model is introduced into the acoustic analogy by a suitable random time shift. In the present paper, the strategy is to compare the capability of CFD tools to model broadband noise sources: therefore, the latter approach is not considered here.

The far field spectra lead to similar conclusions as the wall pressure spectra: the RANS approach only predicts the tonal noise, there is no broadband noise because the turbulent fluctuations are not directly simulated by this approach and since no additional information has been introduced into the far field prediction. The levels of the RANS peaks are higher than the experimental ones, which is not surprising since all the energy is concentrated on small bandwidths. The RANS predicted far field contains many harmonics, since there is no broadband spectrum to out-range them. Conversely, the LES predicts quite well the main Strouhal peak and its width. The broadband spectrum is also fairly well described around the shedding frequency. However, two features are different from the experimental result. First, the LES spectrum contains many jigsaws: this is due to the fact that the computed far field sound spectrum is obtained from one sample whereas the experimental one is averaged from 200 samples. This limitation is due to the use of an explicit time advancement algorithm that requires very small time steps (about 3×10^{-8} s) and consequently increases the computational efforts. Also, the limited duration of the sample (18 cycles) can explain the oscillations observed on the left hand side of the spectrum, because of the limited frequency resolution. The second discrepancy is an over-estimate on the high frequencies of about 10 dB, which exceeds the 5 dB overestimate observed on the wall pressure spectrum (for slightly lower frequencies). Moreover for the wall-pressure, the high frequencies do not

produce a hump as they do in the far field. This could be an error related to the acoustic computation: a possible explanation for this might be that some of the smaller eddies generate spurious sound when they cross the integration surface, the inside part of the eddy being still accounted for as a volume term, the outer part being not taken into account. Thus in certain cases, the dipole cancellation of some quadrupole terms may be momentarily ineffective which could lead to more efficient sources. Apparently this problem does not appear for the large structures when they enter the domain upstream of the leading edge or when they leave it downstream of the trailing edge since the combined RANS/analogy approach has been checked for this, as reported in reference [31]. In order to answer this open question, the volume terms would have to be computed, but this would considerably increase the computational costs and was thus not done in the framework of the present study.

Nevertheless, the present LES allowed to carry out a very good broadband sound computation.

4. CONCLUSIONS

The main conclusions of this study are that LES is able to provide an accurate description of broadband sources of a complex flow, given that high order algorithms and suitable subgrid scale models are used. Even if the cost of such an LES is still very high, a significant reduction can be achieved by choosing implicit time advancement schemes as shown by Sorgüven *et al.* [34], but these have to be applied even more carefully. Another strategy to generalise the use of LES in complex configurations is to develop mixed RANS/LES approaches such as Detached eddy Simulation (DES). Such developments are underway and are currently tested on the rod-airfoil configuration [35]. The present study also shows that the time domain description of turbulent eddies is not only important for the prediction of higher frequency broadband noise, but also for an accurate computation of a statistically steady flow: the LES mean flow results are much more accurate than RANS data obtained with the same solver. Moreover, interactions between random and periodic flow patterns modify the tonal components of radiated sound by broadening their peaks. Finally a comprehensive POD study is a promising post-processing tool for the analysis of broadband noise sources and their interaction with tonal sources.

ACKNOWLEDGEMENTS

The authors thank D. Casalino for his contribution to the LES and the sound computations, and M. Michard and P. Ferrand for their participation to this work. This study was supported by the European Community in the project TurboNoiseCFD G4RD-CT-1999-00144. The CINES provided the parallel computing facilities.

REFERENCES

1. Strouhal, V., Über eine besondere Art der Tonerregung, *Annalen der Physik und Chemie*, 1878, 3(5), 216-251.
2. Wagner, H., Über die Entstehung des dynamischen Auftriebes von tragflügeln, *Zeitschrift für Angewandte Mathematik und Mechanik*, 1925, 5(1), 17-35.

3. Glauert, H., The force and moment on an oscillating airfoil, *British Aeronautical Research Council, Reports & Memoranda*, No. 1242, 1929.
4. Küssner, H.G., Zusammenfassender Bericht über den instationären Auftrieb von Flügeln, *Luftfahrtforschung*, 1936, 13, 410-424.
5. Sears, W.R., Some aspects of non-stationary airfoil theory and its practical application, *Journal of Aeronautical Sciences*, 1941, 8 (3), 104-108.
6. Graham, J.W.S., Similarity rules for thin airfoils in non-stationary subsonic flows, *Journal of Fluid mechanics*, 1970, 43(4), 753-766.
7. Widnall, S., Helicopter noise due to blade-vortex interaction, *Journal of the Acoustical Society of America*, 1971, 51(3), 354-365.
8. Amiet, R.K., High frequency thin airfoil theory for subsonic flow, *American Institute of Aeronautics and Astronautics Journal*, 1976, 14(8), 1076-1082.
9. Amiet, R.K., Low frequency approximations in unsteady small perturbation of subsonic flows, *Journal of Fluid Mechanics*, 1975, 75(3), 545-552.
10. Goldstein, M.E., Atassi, H.M., A complete second order theory for the unsteady flow about an airfoil due to a periodic gust, *Journal of Fluid Mechanics*, 1976, 74(1), 741-765.
11. Terracol, M., Manoha, E., Herrero, C., Sagaut, P., Airfoil noise prediction using large-eddy simulation, Euler equations and Kirchhoff integral, *LES for Acoustics*, Göttingen, 2002.
12. Hanson, D.B., Spectrum of rotor noise caused by atmospheric turbulence, *Journal of the Acoustical Society of America*, 1974, 56 (1), 110-126.
13. Homicz, G.F., George, A.R., Broadband and discrete frequency radiation from subsonic rotors, *Journal of Sound and Vibration*, 1974, 36 (2), 151-177.
14. Majumdar, S.J., Peake, N., Noise generation by the interaction between ingested turbulence and a rotating fan, *Journal of Fluid Mechanics*, 1998, 359, 181-216.
15. Glegg, S., The response of a swept blade row to a 3D gust, *Journal of Sound and Vibration*, 1999, 227(1), 29-64.
16. Boudet, J., *Approches numériques pour la simulation du bruit à large bande en vue de l'application aux turbomachines*, PhD. Thesis, No. d'ordre: 2003-36, Ecole Centrale de Lyon, 2003.
17. Boudet, J., Casalino, D., Jacob, M.C., Ferrand, P., Unsteady RANS computations of the flow past an airfoil in the wake of a rod, *American Society of Mechanical Engineers FEDSM 2002*, paper No. FEDSM2002-31343, Montreal, 2002.
18. Bailly, C., Lafon, P., Candel, S., A stochastic approach to compute noise generation and radiation of free turbulent flows, *American Institute of Aeronautics and Astronautics*, paper 95-092, 1995.
19. Seror, C., Sagaut, P., Bailly, C., Juve, D., On the Radiated Noise computed by Large-Eddy Simulation, *Physics of Fluids*, 2001, 13(2), 476-487.

20. Ffowcs-Williams, J.E., Hawkins, D.L., Sound Generated by Turbulence and Surfaces in Arbitrary Motion, *Philosophical Transactions of the Royal Society*, 1969, A264 (1151), 321-342.
21. Schönwald, N., Li, S.D., Schemel, C., Eschrich, D., Boltalova, N., Thiele, F., Numerical simulation of sound propagation and radiation from aero-engines, *ERCOFTAC Bulletin*, 2003, 58, 55-58.
22. Jacob, M.C., Boudet, J., Casalino, D., Michard, M., A rod-airfoil experiment as benchmark for broadband noise modelling, to appear in *Theoretical and Computational Fluid Dynamics (published online by Springer Verlag)*, 2004.
23. Smati, L., Aubert, S., Ferrand, P., Massao, F., Comparison of numerical schemes to investigate blade flutter, *8th International Symposium on Unsteady Aerodynamics and Aeroelasticity of Turbomachines*, Stockholm, 1997.
24. Erlebacher, G., Hussaini, M.Y., Speziale, C.G., Zang, T.A., Towards the large-eddy simulation of compressible turbulent flows, *Journal of Fluid Mechanics*, 1992, 238, 155-185.
25. Boudet, J., Casalino, D., Jacob, M.J., Ferrand, P., Prediction of sound radiated by a rod using large-eddy simulation, *American Institute of Aeronautics and Astronautics*, AIAA paper 2003-3217, Hilton Head, 2003 (also submitted to *AIAA Journal*).
26. Smagorinsky, J., Numerical study of small-scale intermittency in three-dimensional turbulence, *Monthly Weather Review*, 1963, 91, 99-164.
27. van Driest, E.R., On the turbulent flow near a wall, *Journal of Aeronautical Sciences*, 1956, 23, 1007-1011.
28. Wilcox, D.C., Comparison of two-equation turbulence models for boundary layers with pressure gradient, *American Institute of Aeronautics and Astronautics Journal*, 1993, 31(8), 1414-1421.
29. Casalino, D., An advanced time approach for acoustic analogy predictions, *Journal of Sound and Vibration*, 2003, 261 (4), 583-612.
30. Brentner, K.S., Farassat, F., Analytical comparison of the acoustic analogy and Kirchhoff formulation for moving surfaces, *American Institute of Aeronautics and Astronautics Journal*, 1998, 8 (36), 1379-1386.
31. Casalino, D., Jacob, M., Roger, M., Prediction of rod-airfoil interaction noise using the Ffowcs Williams - Hawkins analogy, *American Institute of Aeronautics and Astronautics Journal*, 2003, 41 (2), 182-191.
32. Williamson, C.H.K., Vortex dynamics in the cylinder wake, *Annual Review of Fluid Mechanics*, 1996, 28, 477-539.
33. Graftieaux, L., Michard, M., Grosjean, N., Combining PIV, POD, and vortex identification algorithms for the study of unsteady turbulent swirling flows, *Measurement Science Techniques*, 2001, 11, 1422-1429.

34. Sorgüven, E. Magagnato, F. & Gabi, M., Sound prediction of an airfoil in the wake of a cylinder, *Proceedings of the Colloquium Euromech 449*, Chamonix, 2003.
35. Greschner, B., Thiele, F., Casalino, D., Jacob, M.C., Influence of turbulence modelling on the broadband noise simulation for complex flows, *American Institute of Aeronautics and Astronautics*, AIAA Paper 2004-2926, Manchester, 2004.